Control Oriented Modelling and Experimental Validation of a PEMFC Generation System

Cristian Kunusch, *Member, IEEE*, Paul F. Puleston, Miguel A. Mayosky, *Senior Member, IEEE*, Attila P. Husar

Abstract—**An experimentally validated control oriented model that reproduces the most typical features of a laboratory Proton Exchange Membrane fuel cell generation system, is presented in this paper. The proposed representation is a 7th order fully analytical nonlinear model of ordinary differential equations, primarily focused on the system gases dynamics. The complete model is developed following a modular procedure, combining theoretical modelling techniques and empirical analysis based on experimental data. The presented methods can be used as a general modelling guideline for control oriented purposes, being possible to adapt to other fuel cell based systems with similar characteristics.**

Index Terms—**Fuel cells systems, control oriented model, nonlinear systems, experimental validation.**

I. INTRODUCTION

Fuel cells represent a radically different approach to energy conversion, one that could replace conventional power generation technologies in a wide variety of applications, from automotive and stationary power systems to portable appliances. In particular, a Proton Exchange Membrane (PEM) fuel cell is an electrochemical device that converts hydrogen chemical energy into electric power energy, without the intermediate production of mechanical work and with water and heat as the only byproducts [1]. Then, considering that hydrogen production from water electrolysis can be performed using renewable energy (solar, wind, geothermal, etc.), PEM fuel cells emerge as one of the cleanest and most promising alternatives to reduce fossil fuel dependency [2].

In this context, improvements in this field require interdisciplinary work and the development of new technologies in many areas. From the automation control point of view, the natural step is to face the challenge of designing and implementing efficient control strategies for the actual fuel cell based energy generation systems. Like in most control design procedures, the first and decisive stage is to obtain a reliable and adequate mathematical description of the system. In this particular case, a control oriented nonlinear model is a key requirement for the development of a control algorithm capable to avoid transient power deterioration and irreversible damages in cell membranes [3].

Furthermore, critical characteristics of PEM fuel cell (PEMFC) based systems such as its viability, robustness and efficiency may be strongly related to their proper control. Hence, several model based control strategies have been reported in the past few years [3][4][5][6][7]. As a matter of fact, modelling PEMFC systems is a particular difficult task, due to the interactions among different subsystems, especially as far as control purposes are concerned. Previous literature models like the ones presented in [8] and [9] are electrochemical characterizations based on empirical relationships that do not consider the dynamics of the different gasses. On the other hand, works such as [3][10][11][12] present extended equations, including gasses dynamics and temperature effects within the stack, however, only [10] and [11] have proposed fully analytical control oriented models. In [11], only a three state air supply subsystem is explained and validated, the humidifier is not included in the model and the characterization of the other subsystems is merely outlined. [10] is probably the first and the most accurate validated control engineering model developed for a PEM fuel cell system, being the base of numerous works such as [3][13][14]. Nevertheless, such accuracy entails a certain degree of complexity, making this model not directly suitable for nonlinear control design.

The goal of the current work is therefore to present a fully validated, fully analytical model of the fuel cell flow dynamics specially developed for nonlinear control purposes. The model retains parameters that have physical significance, so that it can be adapted to other systems. It adequately describes the interaction between the different subsystems (i.e. the fuel cell stack, the reactant supply system and the humidity management unit) from a control point of view.

As a result, based on the use of some general physical laws, the proposed PEMFC control oriented model presents relevant contributions from the automatic control point of view. On the one hand, the systematic procedure developed in the paper makes it a useful general guideline to evaluate other existing modelling schemes and develop new models. On the other hand, the nonlinear control design suitability of the model and the explicit set of state-space equations, make it easy to reproduce and directly apply sophisticated control algorithms, such as Model Predictive Control and Variable Structure Control. It is noteworthy to mention that the authors, using the proposed model, have already obtained encouraging results applying oxygen stoichiometry control by means of homogeneous second order sliding mode design (preliminary results can be found in [15]).

More particularly, the laboratory test plant under study in this proposal mainly comprises a fuel cell stack, an air compressor, a hydrogen storage tank, humidifiers and line heaters (see schematic representation in Fig. 1).

The modelling process is conducted following a modular methodology, combining a theoretical approach, together with empirical analysis based on experimental data. The work is organized in a way such that the fundamentals of the proposed combined methods can be used as a general modelling guideline, being easy to adapt to different fuel cell systems with few
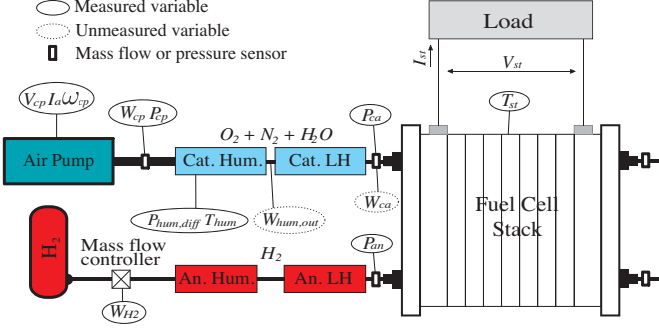
Figure 1. Fuel cell system diagram

modifications. In fact, every subsystem is modelled in terms of physical laws and only adjusting some specific parameters. For instance, following the procedure below, changes in the gas humidification subsystems, the air vacuum pump or even in case of stack replacement would just require to follow the proposed steps and only reprocess some indicated data.

II. AIR COMPRESSOR SUBSYSTEM

The air compressor is a 12V DC oil-free KNF® diaphragm vacuum pump, which is based on a simple principle: an elastic diaphragm, fixed on its perimeter, moves up and down its central point by means of an eccentric. On the down-stroke it draws the air or gas being handled through the inlet valve. On the up-stroke the diaphragm forces the gas through the exhaust valve and out of the head. The compression chamber is hermetically separated from the drive mechanism by the diaphragm. The pump transfers, evacuates and compresses completely oil-free gas and is driven by a 15W DC motor.
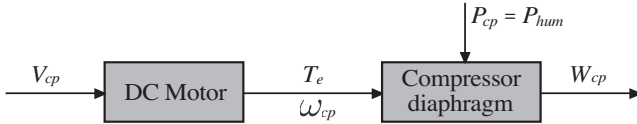

Figure 2. Schematic diagram of the compressor subsystem

The equations that describe the behaviour of the system are obtained by analysing the air compressor as two coupled subsystems. The first one embodies the permanent magnet DC motor dynamics and, the second one, represents the compressing diaphragm nonlinear characteristics (Fig. 2).

A. Air compressor motor dynamic equations

The following equations summarize the dynamic model of the compressor DC motor:

$$V_{cp}(t) = L\frac{di_a(t)}{dt} + Ri_a(t) + k_\phi\omega_{cp}(t) \tag{1}$$

$$J\frac{d\omega_{cp}}{dt} = T_e(t) - T_l(\omega_{cp}(t), P_{cp}(t)) \tag{2}$$

with

$$T_e(t) = k_\phi i_a(t) \tag{3}$$

where V_{cp} is the armature voltage, i_a the armature current, L and R the electrical inductance and resistance of the stator winding, k_ϕ the motor constant, ω_{cp} the shaft angular speed, P_{cp} the absolute pressure at the compressor output, J the inertia, T_e the electrical torque and T_l is a nonlinear function that groups together the effects of the motor and diaphragm friction and the pneumatic load. The computations of the electrical and mechanical parameters of the compressor and the load torque function T_l are developed in a systematic procedure .

To start with, the electrical resistance and inductance of the stator winding can be directly measured through an electronic impedance meter. Then, the k_ϕ value is determined using the electrical equation of the motor (1) in steady state operation:

$$L\frac{di_a(t)}{dt} = V_{cp} - Ri_a - k_\phi\omega_{cp} = 0 \tag{4}$$

From (4), $k_\phi = \frac{V_{cp}-R.i_a}{\omega_{cp}}$ can be computed by measuring i_a and ω_{cp} at different equilibria. Fig. 3 shows that for various compressor pressures (P_{cp}) the value of k_ϕ remains constant.

Figure 3. k_ϕ vs. ω_{cp} (experimental data)
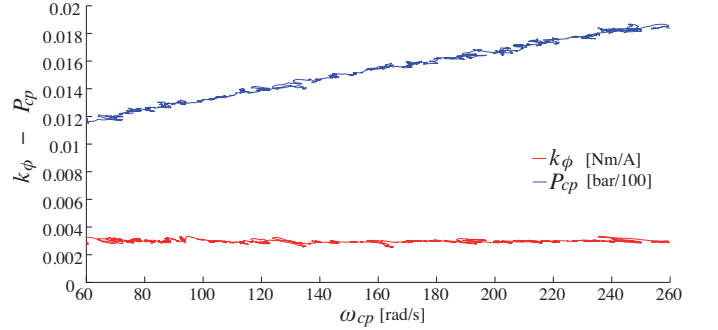
The next step deals with the characterization of the load torque function T_l, that lumps the friction and the pneumatic loads. In a first approach, it can be modelled as a nonlinear static function of ω_{cp} and P_{cp}. For modelling purposes, this load torque expression was divided into two terms:

$$T_l(\omega_{cp}, P_{cp}) = T_{l,amb}(\omega_{cp}) + T'_l(\omega_{cp}, P_{cp}) \tag{5}$$

The former corresponds to the load torque of the system operating at ambient pressure. The latter takes into account the extra torque that appears when the diaphragm vacuum pump operates at pressures higher than the ambient.

The experimental values of the load torque can be computed using data obtained from steady state operation tests. Under these conditions $\dot{\omega}(t)$ is zero, thus equation (2) gives:

$$T_e(t) = k_\phi i_a(t) = T_l(\omega_{cp}, P_{cp}) \tag{6}$$

and T_l can be readily inferred from direct measurement of the current i_a.

Then, with the assistance of (2), the values of the first term of (5), $T_{l,amb}$, are obtained conducting experiments at ambient pressure and different shaft speeds. Analysing the

data (see Fig. 4), it can be concluded that $T_{l,amb}$ can be well approximated by a linear expression, such as:

$$T_{l,amb}(\omega_{cp}) = A_0 + A_1\omega_{cp} \qquad (7)$$

where A_0 and A_1 are parameters determined experimentally that can be found in the Appendix.
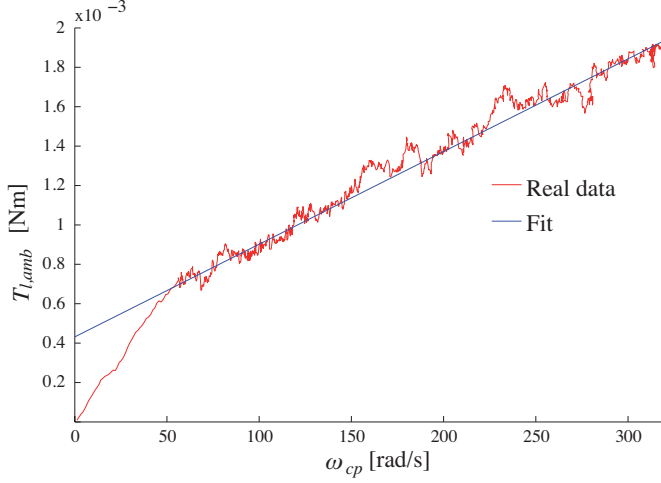

Figure 4. $T_{l,amb}$ vs ω_{cp}: measured data and linear approximation

To find the expression of the second term of (5), T'_l, a new set of experiments is required, with the compressor working at different speeds and compressor pressures, covering its entire range of operation (60 rad/s $< \omega_{cp} <$ 360 rad/s, 1 bar $< P_{cp} <$ 2.5 bar). Then, from (6), (5) and (7), T'_l can be written in terms of the current i_a and the speed ω_{cp}, both measurable variables:

$$\begin{aligned} T'_l(\omega_{cp}, P_{cp}) &= T_l(\omega_{cp}, P_{cp}) - T_{l,amb}(\omega_{cp}) = \qquad (8) \\ &= k_\phi i_a - A_0 - A_1\omega_{cp} \end{aligned}$$

Combining (8) with the data gathered in the experiments, the following bivariate quadratic function can be obtained by means of polynomial regression modelling tools (e.g. polyfitn [16]):

$$\begin{aligned} T'_l &= A_{00} + A_{10}\omega_{cp} + A_{20}\omega_{cp}^2 + A_{01}P_{cp} + \qquad (9) \\ &+ A_{11}\omega_{cp}P_{cp} + A_{02}P_{cp}^2 \end{aligned}$$

with A_{ij} constant coefficients.

In figure 5, two surfaces are displayed. The first one (coloured surface), results from the interpolation of experimental data (dots and crosses). The second one (grey surface), depicts the quadratic approximation (9) that best fits the obtained data.

Note that with this approach, losses due to deviations from the isentropic compression and unmodelled friction terms are now incorporated into the model [10].

The following parameter to be estimated is the motor inertia. Considering the practical impossibility to directly measure J, its value can be determined by adjusting the dynamic response of the model variable $\omega_{cp}(t)$ to the experimental data. In the validation test presented in Fig. 6, step variations are applied
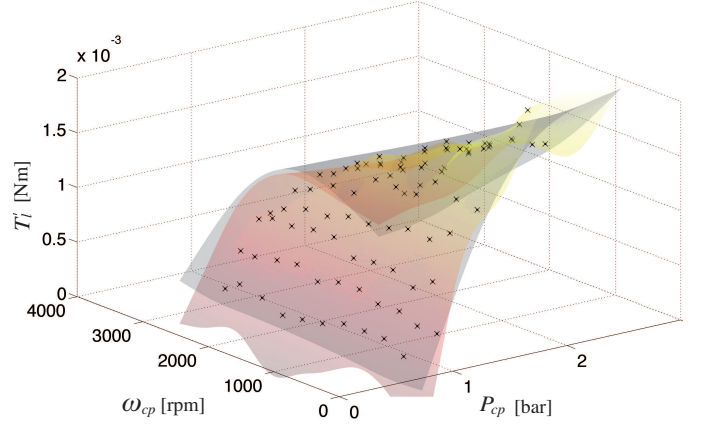

Figure 5. T'_l surface interpolation from real data (coloured surface) and polynomial approximation (grey surface)

to the compressor input voltage. It can be seen that the angular speed matches, even dynamically, the experimental values. This result is verified in a broad span of working conditions, indicating that the developed model is capable to predict the motor behaviour in an extended range of operation. In fact, the approximation error of ω_{cp} remains below 3 % in all the tested working conditions.
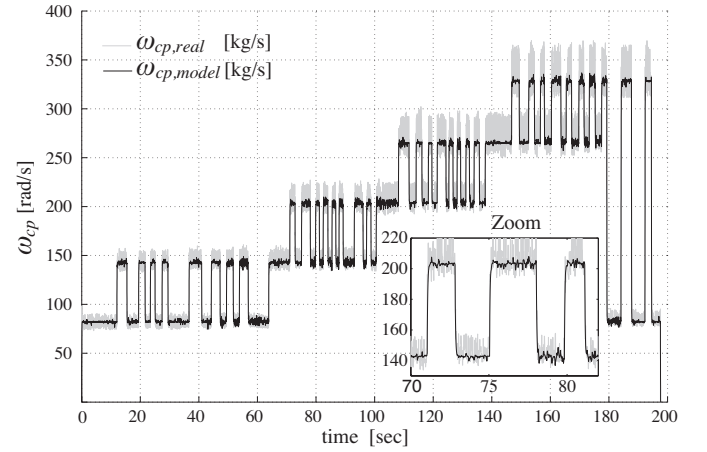

Figure 6. Validation of the DC motor model dynamics

B. Diaphragm vacuum pump characteristics

The next modelling stage required to complete the compressor model is the characterization of the map that relates the output flow W_{cp} with the internal variable ω_{cp} and compressor pressure P_{cp}.

To this end, several steady state tests exploring different operating conditions have been conducted in order to gather data from the mass flow meter, the tachometer and the pressure transducer, respectively. Then, following a fitting procedure similar to the one performed with T'_l, an approximating bivariate function is obtained:

$$\begin{aligned} W_{cp} &= B_{00} + B_{10}\omega_{cp} + B_{20}\omega_{cp}^2 + B_{01}P_{cp} + \qquad (10) \\ &+ B_{11}\omega_{cp}P_{cp} + B_{02}P_{cp}^2 \end{aligned}$$

with B_{ij} constant values.

In figure 7 the W_{cp} approximated surface corresponding to equation (10) is shown (gray surface), as well as the spline interpolation of the real data (coloured surface).
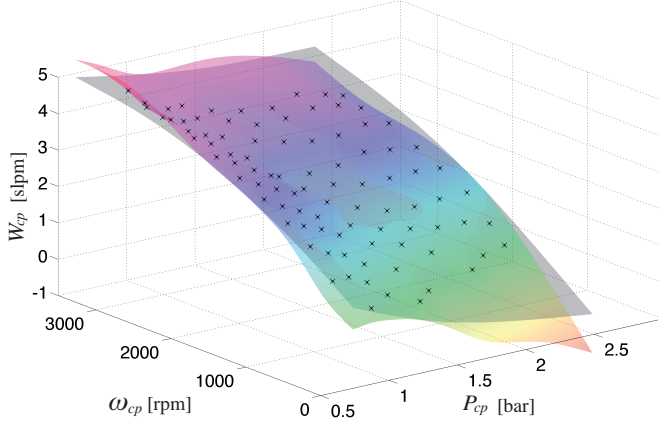

Figure 7. W_{cp} surface interpolation from real data (coloured surface) and polynomial approximation (gray surface)

The parameters and coefficients of the compressor under study can be found in the Appendix.

C. Air compression

The air dynamics corresponding to the compression process inside the diaphragm pump can be fully modelled using the principles of mass and momentum conservation. Nevertheless, a reasonable good approximation from the control viewpoint can be obtained by including this extra dynamics in the motor inertia and readjusting the value of J determined in subsection II.A. The new value of this equivalent inertia is computed from experimental tests and validated in the overall operating range. The obtained value of the gathered inertia (J_g) of the vacuum pump plus the DC motor was $J_g = 1.2$ x 10^{-6} Nm.

Figure 8 presents the time evolution of the compressor air flow of the FC system under consideration. It can be observed that, even during transients, the model provides a very good approximation of the experimental data. This result is also verified at different air compressor flows and pressures.
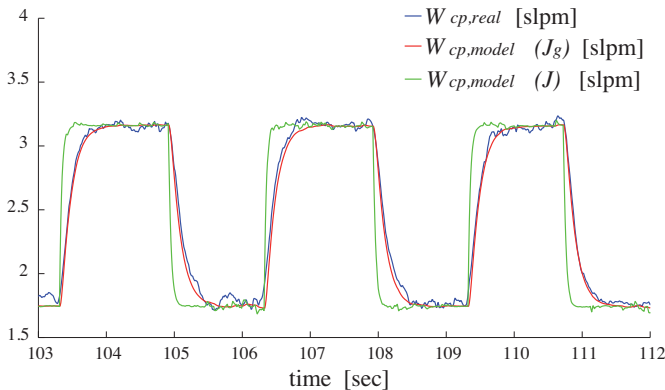

Figure 8. Compressor dynamics

III. AIR HUMIDIFICATION SUBSYSTEM

Cellkraft® P-series humidifiers based on exchange membranes are used to maintain proper humidity conditions inside the cells, which is crucial to ensure the optimal operation of PEM membranes. Gas humidification at flows rates up to 10 slpm and pressures close to 10 bar can be achieved with this sort of devices. The line heaters and stack temperatures are controlled by a power station via decentralized PID controllers, allowing for independent gas conditions to the stack.

The operating principle of the membrane humidification technique is feeding deionized temperature-controlled water and the gas to be humidified to each side of a polymeric membrane, respectively. During the process, a humidity gradient is established across the membrane, allowing the transference of water towards the circulating gas by diffusion. The degree of humidification is regulated by adjusting the water temperature within the humidifier. The closed loop control of moisture can be performed by two different methods, i.e. controlling either the dew point of the gas or the water temperature [17], the temperature control method was implemented for the following experiments.

Prior to entering the stack, the humidified gas circulates through a line heater. The purpose of this device is twofold. On the one hand, by rising the gas temperature, condensation inside the cathode channels is prevented. On the other hand, regulation of the differential temperature (between the humidifier and line heater) allows to control the relative humidity of the cathode inlet gas flow.

To obtain the equations that govern the humidification subsystem, the modelling process is divided into two steps. Firstly, it is assumed that the subsystem dynamics is dominated by the air humidifier pressure change, without taking into account the effect of the vapor injected to the gas (see Figure 9). Then, as a second stage, the effect of the vapor flow injected to the gas is taken into consideration by adding a nonlinear static term, function of the gas temperature, pressure and speed conditions.

Figure 9. Schematic diagram of the humidification subsystem

Step 1:

Under the aforementioned assumptions and considering that the humidifier pressure is the compressor load pressure ($P_{cp} = P_{hum}$), the equations of the cathode humidifier dynamics are given by the following expressions:

$$\frac{dm_{hum}}{dt} = W_{cp} - W_{hum} \qquad (11)$$

$$\frac{dP_{hum}}{dt} = \frac{R_a}{V_{hum}} \left(W_{cp} T_{cp} - W_{hum} T_{hum} \right) \qquad (12)$$

$$W_{hum} = f(T_{hum}, P_{ca}, P_{hum,diff}) \qquad (13)$$

with

$$P_{hum,diff} = P_{hum} - P_{ca} \qquad (14)$$

where m_{hum} and P_{hum} are the mass and pressure of air inside the humidifier, W_{hum} is the flow of air that leaves the humidifier, V_{hum} is the volume of the humidifier, T_{hum} is the gas temperature inside the humidifier, $P_{hum,diff}$ is the humidification subsystem pressure drop and P_{ca} is the cathode inlet pressure.

The right-hand side of (13) corresponds to a non linear nozzle function, strongly dependent on the humidifier gas temperature, the cathode pressure and the humidifier pressure drop (see Fig. 10). It could be approximated by a trivariate function or a family of bivariate functions (parametrised by T_{hum}), obtained through experimental data gathered from tests performed at different operating temperatures and pressures. In particular, the current laboratory test plant is set to operate at constant stack temperature of $60\,^{\circ}\mathrm{C}$ and humidifier temperature of $55\,^{\circ}\mathrm{C}$, respectively, regulated through external controllers. The former is a recommended operation temperature for the equipment, whereas the latter is adjusted to obtain high relative humidity of the cathode inlet flow ($>79\%$), while preventing vapor condensation. Then, considering a constant humidifier working temperature, the nozzle function can be well approximated by the following bivariate function:

$$W_{hum} = C_0 + C_1 P_{hum,diff} P_{ca} + C_2 P_{ca} \qquad (15)$$

where the coefficients C_0, C_1 and C_2 are experimentally determined from the tests (see thick solid lines in Fig. 10).
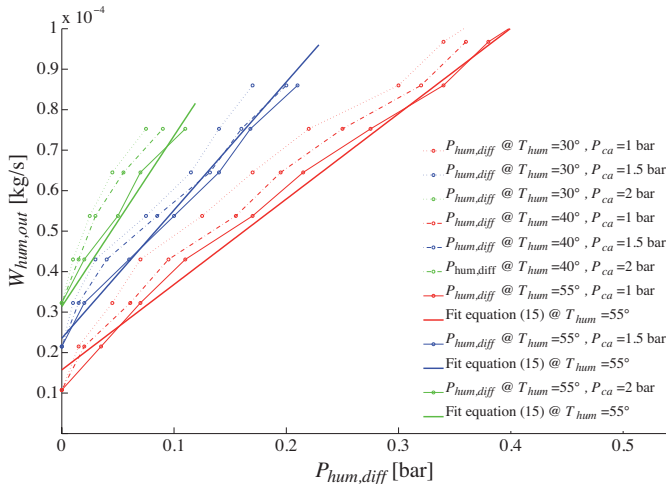

Figure 10.   Humidifier characteristics (fits and real data)

Step 2:

In this step, the vapor injected to the air stream ($W_{v,inj}$) is incorporated to the model. Then, the total humidified air flow entering the cathode (W_{ca}) is given by:

$$W_{ca} = W_{hum} + W_{v,inj} \qquad (16)$$

Assuming that the humidifying closed loop system of the device efficiently regulates the gas relative humidity, the computation of the injected water to the air flow can be described by:

$$W_{v,inj} = \frac{G_v RH_{hum} P_{sat}(T_{hum}) W_{a,hum}}{G_a P_a} - W_{v,hum} \qquad (17)$$

being G_v the vapor molar mass, G_a the dry air molar mass and $P_{sat}(T_{hum})$ the vapor saturation pressure at the humidifier temperature. RH_{hum} is the relative humidity of the gas exiting the humidifier, which in normal operating conditions can be considered a known value, in accordance with the humidifier technical specifications (usually, close to 100%). The dry air partial pressure (P_a), the dry air output flow of the humidifier ($W_{a,hum}$) and the flow of vapor due to ambient moisture entering the humidifier ($W_{v,hum}$), are variables that depend on the ambient conditions and can be directly computed using the following relationships:

$$W_{a,hum} = \frac{1}{1+\omega_{hum}} W_{hum,out} \qquad (18)$$

$$W_{v,hum} = W_{hum} - W_{a,hum} \qquad (19)$$

with

$$\omega_{hum} = \frac{G_v}{G_a} \frac{P_{sat}(T_{amb}) RH_{amb}}{P_{amb} - P_{sat}(T_{amb}) RH_{amb}} \qquad (20)$$

where ω_{hum} is the ambient humidity ratio, T_{amb} the ambient temperature, P_{amb} the ambient pressure and RH_{amb} the ambient relative humidity.

At this point, there is only one parameter left to be estimated to complete the humidification subsystem model. This is the humidifier volume (V_{hum}), present in the dynamic equation (12). An adequate estimation of this parameter can be attained by adjusting the transient response of the modelled P_{hum} to match the experimental data (tests varying the compressor air flow at fixed humidifier temperature are considered). It is important to note that the estimated value does not exactly correspond to the real humidifier volume. It can be interpreted as the volume of an equivalent humidification subsystem, that allows for modelling errors and unmodelled dynamics. Fig. 11 shows that highly satisfactory dynamic validation results are achieved (refer to the Appendix for estimated parameters).

A final remark is pertinent to close this section. It was previously mentioned that regulation of the line heater temperature allows controlling the relative humidity of the gas. Then, in accordance with the Dalton's law, the effect of the increase of temperature (from T_{hum} to T_{lh}) on the partial pressures and the relative humidity of the cathode inlet gas flow can be easily computed through:

$$P_{i,lh} = \frac{T_{lh}}{T_{hum}} P_{i,hum} \qquad (21)$$

$$RH_{lh} = \frac{P_{v,lh}}{P_{sat}(T_{lh})} \qquad (22)$$

where i stands for O_2, N_2 and vapour, respectively, and $P_{sat}(T_{lh})$ is the vapour saturation pressure at the line heater temperature T_{lh}.
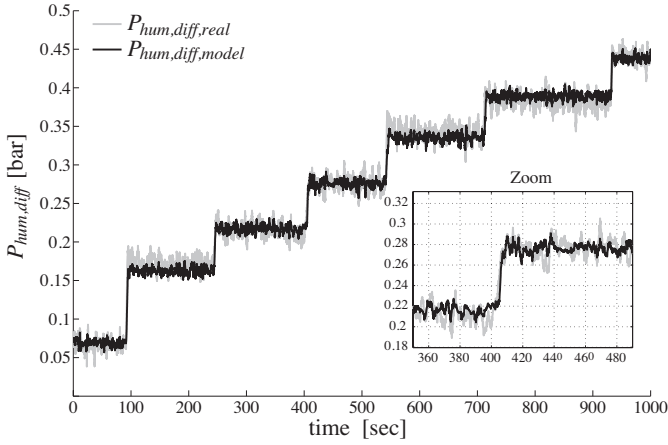
Figure 11. Humidifier dynamic validation

IV. FUEL CELL STACK FLOW SUBSYSTEM

The stack is an EFC50-ST ElectroChem®, which is a laboratory PEM fuel cell system designed for the study of membrane electrode assemblies and fuel cell operation. The system consists of a 7 cell stack with Nafion® 115 membranes, platinum catalyst loading of 1 mg.cm^{-2}, Toray carbon fiber papers as gas diffusion layers and 50 cm^2 of active area. This unit generates 50W under nominal operation conditions and can provide up to 100W peak power during transients.

A. Cathode Channels

The dynamic mass balance within the stack channels depends on the gases partial pressures, on the water transported by the membrane and on the electric current drained from the stack (I_{st}). The cathode state variables are the masses of the circulating elements, i.e. oxygen ($m_{o2,ca}$), nitrogen ($m_{N_2,ca}$) and vapour ($m_{v,ca}$). Then, the dynamic equations that govern the behaviour of the gases inside the cathode are given by:

$$\frac{dm_{o2,ca}}{dt} = W_{o2,ca} - W_{o2,ca,out} - W_{o2,react} \tag{23}$$

$$\frac{dm_{N_2,ca}}{dt} = W_{N_2,ca} - W_{N_2,ca,out} \tag{24}$$

$$\frac{dm_{v,ca}}{dt} = W_{v,ca} - W_{v,ca,out} + W_{v,ca,gen} + W_{v,mem} \tag{25}$$

while the following relationships hold for the cathode input and output flows (W_{ca} and $W_{ca,out}$):

$$W_{ca} = W_{o2,ca} + W_{N_2,ca} + W_{v,ca} \tag{26}$$

$$W_{ca,out} = W_{o2,ca,out} + W_{N_2,ca,out} + W_{v,ca,out} \tag{27}$$

being $W_{o2,ca}$, $W_{N_2,ca}$, $W_{v,ca}$, $W_{o2,ca,out}$, $W_{N_2,ca,out}$ and $W_{v,ca,out}$ the input and output flows of oxygen, nitrogen and vapour, $W_{o2,react}$ the flow of oxygen that reacts in the cathode, $W_{v,ca,gen}$ the flow of vapour generated in the reaction and $W_{v,mem}$ the flow of water transferred across the membrane (comprising an electro-osmotic drag term and a back-diffusion term).

Subsequently, the calculation of the flow terms that constitute the right-hand sides of equations (23)-(25) must be addressed.

To begin with, the amount of reduced oxygen and generated vapour in the cathode reaction is computed from the stack current, according to the following two electrochemical principles:

$$W_{o2,react} = G_{o2} \frac{nI_{st}}{4F} \tag{28}$$

$$W_{v,ca,gen} = G_v \frac{nI_{st}}{2F} \tag{29}$$

where n is the number of cells of the stack, G_{o2} and G_v are the molar masses of oxygen and vapour, respectively, and F is the Faraday constant.

Next, the components of the cathode input and output flows are considered. Firstly, assuming knowledge of W_{ca} from (16), the partial input flows $W_{o2,ca}$, $W_{N_2,ca}$ and $W_{v,ca}$ are readily calculated using (26):

$$W_{o2,ca} = X_{o2,ca} \frac{1}{1+\omega_{ca}} W_{ca} \tag{30}$$

$$W_{N_2,ca} = (1 - X_{o2,ca}) \frac{1}{1+\omega_{ca}} W_{ca} \tag{31}$$

$$W_{v,ca} = W_{ca} - W_{N_2,ca} - W_{o2,ca} \tag{32}$$

where ω_{ca} is the humidity ratio and $X_{o2,ca}$ the mass mole fraction of the input air flow, given by:

$$\omega_{ca} = \frac{G_v P_{v,lh}}{G_a(P_{o2,lh} + P_{N_2,lh})} \tag{33}$$

$$X_{o2,ca} = \frac{y_{o2,amb} G_{o2}}{y_{o2,amb} G_{o2} + (1 - y_{o2,amb}) G_{N_2}} \tag{34}$$

being $y_{o2,amb}$ the ambient oxygen mole fraction.

Secondly, using (27), the partial output flows $W_{o2,ca,out}$, $W_{N_2,ca,out}$ and $W_{v,ca,out}$ can be obtained following a similar procedure:

$$W_{o2,ca,out} = X_{o2,ca,out} \frac{1}{1+\omega_{ca,out}} W_{ca,out} \tag{35}$$

$$W_{N_2,ca,out} = (1 - X_{o2,ca,out}) \frac{1}{1+\omega_{ca,out}} W_{ca,out} \tag{36}$$

$$W_{v,ca,out} = W_{ca,out} - W_{o2,ca,out} - W_{N_2,ca,out} \tag{37}$$

with the output humidity ratio and mass mole fraction:

$$\omega_{ca,out} = \frac{G_v P_{v,ca}}{G_a(P_{o2,ca} + P_{N_2,ca})} \tag{38}$$

$$X_{o2,ca,out} = \frac{y_{o2,out} G_{o2}}{y_{o2,out} G_{o2} + (1 - y_{o2,out}) G_{N_2}} \tag{39}$$

$$y_{o2,out} = \frac{P_{o2}}{P_{ca}} \tag{40}$$

with $y_{o2,out}$ the cathode oxygen mole fraction.

However, for these computations the cathode output flow $W_{ca,out}$ is not yet available, given that it is not measurable due to its high vapour content. It must be indirectly obtained,

making use of the pressure drop measurement. The relationship between the output flow and the pressure drop can be modelled as a linear nozzle equation:

$$W_{ca,out} = K_{ca,out}(P_{ca} - P_{rm,ca}) \quad (41)$$

where $P_{rm,ca}$ is the return manifold pressure, governed through a mechanical back pressure regulator.

Then, to compute $W_{ca,out}$ it is necessary to determine $K_{ca,out}$. To estimate this parameter, experimental data of the pressure drop and the cathode output flow is required. The former is available from the differential pressure transducer but, as it was previously said, no direct measurement of $W_{ca,out}$ is feasible due to its high relative humidity. However, under appropriate experimental conditions, its steady state values can be inferred from measurements of the compressor flow W_{cp}. The estimation test conditions are: (a) steady state operation, (b) equally humidified reactant gases and (c) nil stack current. On the one hand, $I_{st} = 0$ guarantees that the liquid water ($W_{l,ca,out}$) and the reaction flows ($W_{o_2,react}$ and $W_{v,ca,gen}$) remain zero. On the other hand, considering anode and cathode gases at similar relative humidities ensures that at steady state operation there is no water concentration gradient across the membrane, so the effect of $W_{v,mem}$ can be neglected. Therefore, under these testing conditions $W_{ca,out}$ is equal to W_{ca} (see (23)-(25)). Then, using (11), (16) and (17), data of W_{cp} allows the computation of $W_{ca,out}$ and, consequently, the estimation of the nozzle restriction.

Note that the partial pressures of the gases inside the cathode, required in (33), can be obtained from the stack temperature and the masses of oxygen, nitrogen and vapour. Using the Dalton's law, the cathode partial pressures and relative humidity are:

$$P_{i,ca} = \frac{m_{i,ca} R_i T_{st}}{V_{ca}} \quad (42)$$

$$RH_{ca} = \frac{P_{v,ca}}{P_{sat}(T_{st})} \quad (43)$$

where subscript i stands for O_2, N_2 and v, respectively, and V_{ca} is the cathode volume.

The last flow term of (23)-(25) to be computed is the water transferred across the membrane. To this end, the anode relative humidity is required, so the anode flow model will be firstly addressed and, subsequently, the calculation of $W_{v,mem}$ will be resumed.

B. Anode Channels

In this type of PEMFC systems the input hydrogen flow is independently regulated, thus it is assumed as a known constant input W_{an}. Under this conditions the dynamics of the anode channel can be modelled by:

$$\frac{dm_{H_2,an}}{dt} = W_{H_2,an} - W_{H_2,an,out} - W_{H_2,react} \quad (44)$$

$$\frac{dm_{v,an}}{dt} = W_{v,an} - W_{v,an,out} - W_{v,mem} \quad (45)$$

while the following equations hold for the anode input and output flows:

$$W_{an} = W_{H_2,an} + W_{v,an} \quad (46)$$

$$W_{an,out} = W_{H_2,an,out} + W_{v,an,out} \quad (47)$$

being $W_{H_2,an}$, $W_{v,an}$, $W_{H_2,ca,out}$ and $W_{v,an,out}$ the input and output flows of hydrogen and vapour, respectively, $W_{H_2,react}$ the flow of hydrogen consumed in the reaction and $W_{v,mem}$ the aforementioned flow of water transferred to the cathode. In this particular case, no liquid water is supposed to be condensed in the anode channels, given that in normal working conditions the relative humidity of the anode is always below 100%. On the other hand, the hydrogen consumed in the reaction is:

$$W_{H_2,react} = G_{H_2} \frac{n I_{st}}{2F} \quad (48)$$

where G_{H_2} stands for the molar mass of hydrogen.

Analogously to the cathode channel, the components of the anode input and output flows must be calculated. The partial input flows $W_{H_2,an}$ and $W_{v,an}$ are obtained through:

$$W_{H_2,an} = \frac{1}{1 + \omega_{an}} W_{an} \quad (49)$$

$$W_{v,an} = W_{an} - W_{H_2,an} \quad (50)$$

$$\omega_{an} = \frac{G_v P_{v,lh,an}}{G_{H_2} P_{H_2,lh,an}} \quad (51)$$

where ω_{an} is the humidity ratio of the anode input gas, $P_{lh,an}$ the anode input pressure and $P_{v,lh,an}$ the anode input vapour pressure, that can be obtained using the Dalton's law.

Besides, the partial output flows $W_{H_2,an,out}$ and $W_{v,an,out}$ are computed as follows:

$$W_{H_2,an,out} = \frac{1}{1 + \omega_{an,out}} W_{an,out} \quad (52)$$

$$W_{v,an,out} = W_{an,out} - W_{H_2,an,out} \quad (53)$$

$$\omega_{an,out} = \frac{G_v P_{v,an}}{G_{H_2} P_{H_2,an}} \quad (54)$$

where $\omega_{an,out}$ is the humidity ratio of the gas inside the anode, P_{an} the anode pressure and $P_{v,an}$ the anode vapour pressure.

C. Membrane Water Transport

Now the calculation of $W_{v,mem}$ can be taken up again. The flow of water across the membrane is modelled assuming linear concentration gradients from channels inlet to outlet and across the membrane thickness. Then, it can be expressed as [9]:

$$W_{v,mem} = \left[n_d \frac{i}{F} + D_w \frac{c_{v,ca} - c_{v,an}}{t_m} \right] G_v A_{fc} n \quad (55)$$

where i is the stack current density, A_{fc} the fuel cell active area, t_m the membrane dry thickness and $c_{v,ca}$ and $c_{v,an}$ the water concentration at the membrane surfaces on the cathode

and anode sides respectively. The term n_d is the electro-osmotic drag coefficient (number of water molecules carried by each proton) and D_w the back-diffusion coefficient of the membrane. The water concentration terms are determined from the membrane water contents on the cathode (λ_{ca}) and anode (λ_{an}) sides:

$$c_{v,ca} = \frac{\rho_{m,dry}}{G_{m,dry}} \lambda_{ca} \tag{56}$$

$$c_{v,an} = \frac{\rho_{m,dry}}{G_{m,dry}} \lambda_{an} \tag{57}$$

where $\rho_{m,dry}$ is the membrane dry density and $G_{m,dry}$ the membrane dry molecular weight. The water content in the membrane is defined as the ratio of water molecules to the number of charge sites. When no liquid water is present in the channels, the ratio can be estimated at both sides using the following equation [9]:

$$\lambda_j = a_0 + a_1 RH_j + a_2 RH_j^2 + a_3 RH_j^3 \tag{58}$$

being RH_j the gas relative humidity and subscript j referring to cathode or anode ($j = ca, an$), respectively.

The next step is to estimate the apparent diffusion coefficient D_w of expression (55). Two different experiments can be set-up to compute this parameter, either a cathode or an anode drying test. In both cases, the stack current must be set to zero (I_{st}=0) in order to cancel the stack current density i in (55). For the former, a long term cathode drying procedure is conducted, decreasing the cathode humidifier temperature from $55\,^{\circ}\text{C}$ to $40\,^{\circ}\text{C}$, while setting the temperatures of the anode humidifier, both line heaters and the stack at $60\,^{\circ}\text{C}$. With this test, a water concentration gradient is established between the channels and an increasing extra flow in the cathode output can be detected due to the membrane contribution.

The second test is conducted analogously to the first one, but in this case the anode channel is dried out, keeping the other variables at similar stationary conditions. Following this simple procedure, the D_w coefficient can be directly determined without using humidity sensors or a more specific equipment. Figure 12 displays the data gathered from both tests (the average value obtained for the back-diffusion coefficient is given in the Appendix).
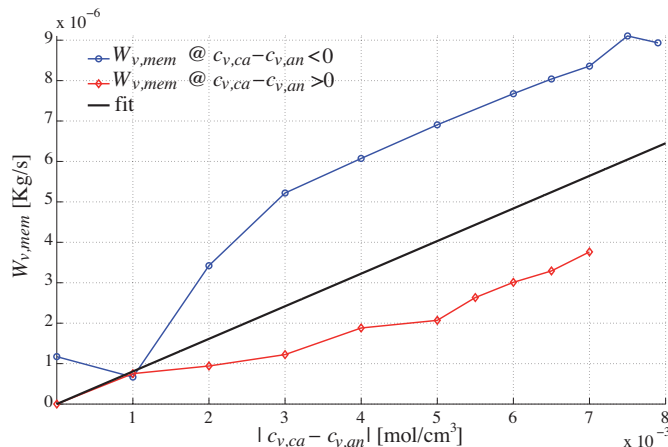

Figure 12. Experimental and estimated membrane water diffusion characterisation

Finally, the electro-osmotic coefficient n_d is characterised through the widely accepted expression developed in [18] and reported in [3] and [19]:

$$n_d = n_0 + n_1 \lambda_m + n_2 \lambda_m^2 \tag{59}$$

where λ_m is the average membrane water content, which can be derived from equation (58) considering:

$$RH_m = (RH_{ca} + RH_{an})/2 \tag{60}$$

V. Control Oriented State Space Model

The final modelling phase, previous to the controller design stage, deals with the rearrangement of the equations presented in sections II-IV, in order to obtain an state space model, suitable for nonlinear control design purposes. This procedure comprises both, coupling all the presented differential equations with its auxiliary equations in order to represent the system only in terms of the space states, external inputs (I_{st}, $W_{an,in}$ and V_{cp}) and constants, as well as taking into account any possible assumptions that lead to order reduction. In this particular case, the latter assumptions involve taking $T_{cp} = T_{hum}$ and $di_a/dt = 0$, which in turn, are assumptions based on different tests that have revealed that the equations (11-12) are linearly coupled within the PEMFC operating range and the time constant of the variable I_{st} can be neglected respect to the rest of the system dynamics. Another possible assumption that can be performed in these type of PEMFC systems is to consider the anode line dynamics decoupled with the cathode line, because its only interaction depend on the term $W_{v,mem}$. Further information about how the overall state space equations were obtained can be found in [2].

Then, taking state $x \in \mathbb{R}^7$, control input $u = V_{cp} \in \mathbb{R}^1$ and the operating conditions given in Table V of the appendix, the PEMFC generation system under study can be described in the form $\dot{x} = f(x, I_{st}) + g.u$, accordingly to the following set of state space equations (61-67):

VI. Conclusions

The control oriented model derived in this paper reproduces the most typical features of a laboratory PEM fuel cell arrangement, which is a complex system that combines mechanical, electrical, pneumatic and electrochemical subsystems. The proposed representation is a 7th order nonlinear model primarily focused on the fuel cell fluid dynamics, presenting the following features, required for control design: continuous, smooth dynamic vector fields and bounded uncertainty. The complete model in state-space representation is presented and discussed considering modular subsystems. It is important to stress that the presented model validation covers the entire operation range of the fuel cell based system under study, even though an overall test could not be displayed due to space limitations.

Important control problems found in PEM fuel cells such as the ones presented in [5][3][10] and [20] (H_2/O_2 stoichiometry regulation, total and partial pressures control, H_2 consumption minimization, etc.), can be approached using the developed control model.

$$\dot{x}_1 = \left(m_1 \left(u(t) - m_2 x_1 \right) - x_1 m_3 + A_0 + A_{00} + A_{10} \left(x_2 m_5 + m_6 \right) + \right.$$
$$\left. + \; A_{20} \left(x_2 m_5 + m_6 \right)^2 + A_{01} x_1 + A_{11} \left(x_2 m_5 + m_6 \right) x_1 + A_{02} x_1^2 \right) m_4 \tag{61}$$

$$\dot{x}_2 = B_{00} + B_{10} \left(x_2 \, m_5 + m_6 \right) + B_{20} \left(x_2 \, m_5 + m_6 \right)^2 + B_{01} \, x_1 +$$
$$+ \; B_{11} \left(x_2 \, m_5 + m_6 \right) x_1 + B_{02} \, x_1^2 - b_1(x)^3 C_3 - b_1(x)^2 C_2 - b_1(x) \, C_1 - C_0 \tag{62}$$

$$\dot{x}_3 = \left(m_9 \left(b_1(x)^3 C_3 + b_1(x)^2 C_2 + b_1(x) \, C_1 + C_0 \right) G_a^{-1} \left(x_2 \, m_5 - m_{10} \right)^{-1} \right.$$
$$\left(1 + \frac{m_{11}}{x_2 \, m_5 - m_{10}} \right)^{-1} + \left(b_1(x)^3 C_3 + b_1(x)^2 C_2 + b_1(x) \, C_1 + C_0 \right)$$
$$\left(1 + \frac{m_{11}}{x_2 \, m_5 - m_{10}} \right)^{-1} X_{o2,ca,in} \left(1 + \frac{m_{14}}{(x_3 \, R_{o2} + x_4 \, R_{N2} + x_5 \, R_v) \, m_8 - m_{12}} \right)^{-1} -$$
$$- \; K_{ca} \left((x_3 \, R_{o2} + x_4 \, R_{N2} + x_5 \, R_v) \, m_8 - P_{amb} \right) x_3 \, R_{o2} \, G_{o2}$$
$$\left(1 + G_v \, x_5 \, R_v \left(\frac{x_3 \, R_{o2} \, G_{o2}}{x_3 \, R_{o2} + x_4 \, R_{N2}} + \left(1 - \frac{x_3 \, R_{o2}}{x_3 \, R_{o2} + x_4 \, R_{N2}} \right) G_{N2} \right)^{-1} \right.$$
$$\left. \left(x_3 \, R_{o2} + x_4 \, R_{N2} \right)^{-1} \right)^{-1} \left(x_3 \, R_{o2} + x_4 \, R_{N2} \right)^{-1}$$
$$\left(\frac{x_3 \, R_{o2} \, G_{o2}}{x_3 \, R_{o2} + x_4 \, R_{N2}} + \left(1 - \frac{x_3 \, R_{o2}}{x_3 \, R_{o2} + x_4 \, R_{N2}} \right) G_{N2} \right)^{-1} - 1/4 \, \frac{G_{o2} \, n I_{st}}{F} \tag{63}$$

$$\dot{x}_4 = \left(m_9 \left(b_1(x)^3 C_3 + b_1(x)^2 C_2 + b_1(x) \, C_1 + C_0 \right) G_a^{-1} \left(x_2 \, m_5 - m_{10} \right)^{-1} \right.$$
$$\left(1 + \frac{m_{11}}{x_2 \, m_5 - m_{10}} \right)^{-1} + \left(b_1(x)^3 C_3 + b_1(x)^2 C_2 + b_1(x) \, C_1 + C_0 \right)$$
$$\left(1 + \frac{m_{11}}{x_2 \, m_5 - m_{10}} \right)^{-1} \left(1 - X_{o2,ca,in} \right) \left(1 + \frac{G_v \, m_{12}}{G_a \, (b_2(x) - m_{12})} \right)^{-1} -$$
$$- \; \left(1 - x_3 \, m_8 \, G_{o2} \, b_3(x)^{-1} \left(\frac{x_3 \, m_8 \, G_{o2}}{b_3(x)} + \left(1 - \frac{x_3 \, m_8}{b_3(x)} \right) G_{N2} \right)^{-1} \right)$$
$$K_{ca,n} \left(b_2(x) - P_{amb} \right) \left(1 + G_v \, x_5 \, R_v \, m_8 \left(\frac{x_3 \, m_8 \, G_{o2}}{b_3(x)} + \left(1 - \frac{x_3 \, m_8}{b_3(x)} \right) G_{N2} \right)^{-1} \right.$$
$$\left. \left(x_3 \, R_{o2} \, m_8 + x_4 \, R_{N2} \, m_8 \right)^{-1} \right)^{-1} \tag{64}$$

$$\dot{x}_5 = G_v \, m_{12} \left(b_1(x)^3 C_3 + b_1(x)^2 C_2 + b_1(x) \, C_1 + C_0 \right) G_a^{-1} \left(x_2 \, m_5 - m_{10} \right)^{-1}$$
$$\left(1 + \frac{G_v \, m_{10}}{G_a \, (x_2 \, m_5 - m_{10})} \right)^{-1} + \frac{b_4(x)}{b_5(x)} - \left(\frac{G_v \, m_{12} \, b_4(x)}{G_a \, (x_2 \, m_5 - m_{10}) \, b_5(x)} + \frac{b_4(x)}{b_5(x)} \right)$$
$$\left(1 + \frac{G_v \, m_{12}}{G_a \, (b_2(x) - m_{12})} \right)^{-1} - K_{ca,out} \left(b_2(x) - P_{amb} \right) + K_{ca,out} \left(b_2(x) - P_{amb} \right)$$
$$\left(1 + G_v \, x_5 \, R_v \, m_8 \, b_3(x)^{-1} \left(\frac{x_3 \, m_8 \, G_{o2}}{b_3(x)} + \left(1 - \frac{x_3 \, m_8}{b_3(x)} \right) G_{N2} \right)^{-1} R_{o2}^{-1} \right)^{-1}$$
$$+ \; 1/2 \, \frac{G_v \, n I_{st}}{F} + \left(\left(n_0 + n_1 \left(a_0 + a_1 \, b_6(x) + a_2 \, b_6(x)^2 + a_3 \, b_6(x)^3 \right) + \right. \right.$$
$$+ \; n_2 \left(a_0 + a_1 \, b_6(x) + a_2 \, b_6(x)^2 + a_3 \, b_6(x)^3 \right)^2 \right) I_{st}/A_{fc}/F -$$
$$- \; D_w \left(\frac{\left(a_0 + a_1 \, x_5 \, m_{16} + a_2 \, x_5^2 m_{16}^2 + a_3 \, x_5^3 m_{16}^3 \right) \rho_{m,dry}}{G_{m,dry}} - \right.$$
$$- \; \left. \left. \frac{\left(a_0 + a_1 \, x_7 \, m_{15} + a_2 \, x_7^2 m_{15}^2 + a_3 \, x_7^3 m_{15}^3 \right) \rho_{m,dry}}{G_{m,dry}} \right) t_m^{-1} \right) G_v \, A_{fc} \, n \tag{65}$$

$$\dot{x}_6 = W_{an,in} \left(1 + \frac{G_v \, m_{17}}{G_{H_2} \, (b_7(x) - m_{17})} \right)^{-1} - K_{an,out} \left(b_7(x) - P_{amb} \right) \left(1 + \frac{G_v \, x_7 \, m_{19}}{G_{H_2} \, x_6 \, m_{20}} \right)^{-1}$$
$$- \; 1/2 \, \frac{G_{H_2} \, n I_{st}}{F} \tag{66}$$

$$\dot{x}_7 = W_{an,in} - W_{an,in} \left(1 + \frac{G_v \, m_{17}}{G_{H_2} \, (b_7 - m_{17})} \right)^{-1} - K_{an,out} \left(b_7(x) - P_{amb} \right)$$
$$+ \; K_{an,out} \left(b_7(x) - P_{amb} \right) \left(1 + \frac{G_v \, x_7 \, m_{19}}{G_{H_2} \, x_6 \, m_{20}} \right)^{-1} -$$
$$- \; \left(\left(n_0 + n_1 \left(a_0 + a_1 \, b_6(x) + a_2 \, b_6(x)^2 + a_3 \, b_6(x)^3 \right) + \right. \right.$$
$$+ \; n_2 \left(a_0 + a_1 \, b_6(x) + a_2 \, b_6(x)^2 + a_3 \, b_6(x)^3 \right)^2 \right) I_{st}/A_{fc}/F -$$
$$- \; D_w \left(\frac{\left(a_0 + a_1 \, x_5 \, m_{16} + a_2 \, x_5^2 m_{16}^2 + a_3 \, x_5^3 m_{16}^3 \right) \rho_{m,dry}}{G_{m,dry}} - \right.$$
$$- \; \left. \left. \frac{\left(a_0 + a_1 \, x_7 \, m_{15} + a_2 \, x_7^2 m_{15}^2 + a_3 \, x_7^3 m_{15}^3 \right) \rho_{m,dry}}{G_{m,dry}} \right) t_m^{-1} \right) G_v \, A_{fc} \, n \tag{67}$$

The mixed methodology used in this paper is not an example on identification nor a theoretical exercise. Guided by the knowledge of the processes and reactions that take place in the real fuel cell system, the different components were modelled using available information and simple experiments. Therefore, the proposed strategy can be used as a general guide for control oriented modelling in PEM fuel cell systems with similar features. Moreover, the reactant flow model developed in this work can be successfully complemented with the work developed by the authors in a recent publication [21], where a complete characterization of the stack output voltage in terms of its operating conditions (flows, pressures, current densities) was presented.

Due to the fact that the model was primarily developed for model based control studies, a system level approach was considered and only dynamic effects with time constants in the range of 10^{-2} sec. to 10^{0} sec. were taken into account.

The developed nonlinear model accurately describes the steady state and dynamical behaviour of the studied fuel cell stack and its associate devices.

APPENDIX

Auxiliary functions

$$b_1(x) = x_3\, m_5 - (x_4\, R_{O_2} + x_5\, R_{N_2} + x_6\, R_v)\, m_8$$

$$b_2(x) = (x_4\, R_{O_2} + x_5\, R_{N_2} + x_6\, R_v)\, m_8$$

$$b_3(x) = \frac{x_4\, R_{O_2}\, m_8 + x_5\, R_{N_2}\, m_8}{R_{O_2}}$$

$$b_4(x) = C_0 + C_1\, b_1(x)\, b_2(x) + C_2\, b_2(x)$$

$$b_5(x) = 1 + \frac{G_v\, m_{10}}{G_a\,(x_3\, m_5 - m_{10})}$$

$$b_6(x) = \frac{x_8\, m_{15}}{2} + \frac{x_6\, m_{16}}{2}$$

$$b_7(x) = (x_7\, R_{H_2} + x_8\, R_v)\, m_{18}$$

Tables

Parameter	Value
Electrical inductance (L)	2.12 mH
Electrical resistance (R)	2.03 Ω
Torque constant (k_ϕ)	0.0031 Nm/A
Motor inertia (J)	2 x 10^{-7} Nm
Compressor gathered inertia (J_g)	1.2 x 10^{-6} Nm
Load torque coefficient (A_0)	4.10 x 10^{-4} Nm
Load torque coefficient (A_1)	3.92 x 10^{-6} Nms

Table I
COMPRESSOR PARAMETERS

Parameter	Value
Air gas constant (R_a)	286.9 Nm/kg/°K
Vapour molar mass (G_v)	0.01802 kg/mol
Dry air molar mass (G_a)	0.029 kg/mol
Oxygen molar mass (G_{o_2})	32 x 10^{-3} kg/mol
Nitrogen molar mass (G_{N_2})	28 x 10^{-3} kg/mol
Hydrogen molar mass (G_{H_2})	2.01 x 10^{-3} kg/mol
Air gas constant (R_a)	286.9 Nm/kg/°K
Oxygen gas constant (R_{o_2})	259.8 Nm/kg/°K
Nitrogen gas constant (R_{N_2})	296.8 Nm/kg/°K
Vapour gas constant (R_v)	461.5 Nm/kg/°K
Hydrogen gas constant (R_{H_2})	4.124 x 10^3 Nm/kg/°K
Faraday constant (F)	96485 C/mol

Table II
GENERAL PHYSICAL CONSTANTS

Parameter	Value
A_{00}	0
A_{10}	0.0058 Nms
A_{20}	-0.0013 Nms^2
A_{01}	3.25 x 10^{-6} Nm/bar
A_{11}	-2.80 x 10^{-6} Nms/bar
A_{02}	-1.37 x 10^{-9} Nms/bar^2
B_{00}	4.83 x 10^{-5} kg/s
B_{10}	-5.42 x 10^{-5} kg/s^2
B_{20}	8.79 x 10^{-6} kg/s^3
B_{01}	3.49 x 10^{-7} kg/s^2/bar
B_{11}	3.55 x 10^{-13} kg/s
B_{02}	-4.11 x 10^{-10} kg/s/bar

Table III
POLYNOMIAL COEFFICIENTS OF EQUATIONS (10) AND (11)

Parameter	Value
Humidifier temperature (T_{hum})	55 °C
Line heater temperature (T_{lh})	60 °C
Fuel cell stack temperature (T_{st})	60 °C
Humidifier relative humidity (RH_{hum})	0.95
Ambient relative humidity (RH_{amb})	0.5
Ambient pressure (P_{amb})	1 bar
Ambient temperature (T_{amb})	25 °C
Ambient oxygen mole fraction ($y_{o_2,amb}$)	25 °C
Hydrogen input flow ($W_{H_2,an}$)	2 slpm

Table IV
OPERATING CONDITIONS

Parameter	Value
Humidifier volume (V_{hum})	2 x 10^{-4} m^3
Humidifier restriction coefficient (C_0)	1.048 x 10^{-7} kg/s
Humidifier restriction coefficient (C_1)	2.109 x 10^{-4} kg/s/bar^2
Humidifier restriction coefficient (C_2)	1.562 x 10^{-5} kg/s/bar
Number of fuel cells (n)	7
Cathode restriction constant ($K_{ca,out}$)	0.0094 kg/s/bar
Cathode volume (V_{ca})	4 x 10^{-4} m^3
Membrane effective area (A_{fc})	50 cm^2
Membrane dry thickness (t_m)	0.0127 cm
Membrane dry density ($\rho_{m,dry}$)	0.002 kg/cm^3
Membrane dry molecular weight ($G_{m,dry}$)	1.1 kg/mol
Membrane diffusion coefficient (D_w)	5.43 x 10^{-6} cm^2/s
Membrane water content coefficient (a_0)	0.043 [H_2O/SO_3]
Membrane water content coefficient (a_1)	17.81 [H_2O/SO_3]
Membrane water content coefficient (a_2)	-39.85 [H_2O/SO_3]
Membrane water content coefficient (a_3)	36.0 [H_2O/SO_3]
Electro-osmotic coefficient (n_0)	-3.4x10^{-19} [H_2O/H^+]
Electro-osmotic coefficient (n_1)	0.05 [H_2O/H^+]
Electro-osmotic coefficient (n_2)	0.0029 [H_2O/H^+]

Table V
AIR HUMIDIFIER AND FUEL CELL STACK PARAMETERS

$m_1 = k_\phi/R$
$m_2 = k_\phi 30/\pi$
$m_3 = A_1 30/\pi$
$m_4 = \pi/30/J$
$m_5 = T_{sm} R_a/V_{hum}$
$m_6 = -P_{sat}(T_{sm})RH_{amb} + RH_{hum,ca}P_{sat}(T_{hum,ca})$
$m_8 = T_{st}/V_{ca}$
$m_9 = G_v RH_{hum,ca} P_{sat}(T_{hum,ca})$
$m_{10} = P_{sat}(T_{sm})\ RH_{amb}$
$m_{11} = G_v P_{sat}(T_{sm})RH_{amb}/G_a$
$m_{12} = RH_{hum,ca}P_{sat}(T_{hum,ca})$
$m_{13} = R_o T_{st} G_O$
$m_{14} = G_v RH_{hum,ca} P_{sat}(T_{hum,ca})/G_{a,ca,in}$
$m_{15} = T_{st} R_v/V_{an}/P_{sat}(T_{lh,an})$
$m_{16} = R_v T_{st}/V_{ca}/P_{sat}(T_{lh,ca})$
$m_{17} = RH_{an,in}P_{sat}(T_{lh,an})$
$m_{18} = T_{st}/V_{an}$
$m_{19} = T_{st} R_v/V_{an}$
$m_{20} = T_{st} R_h/V_{an}$

Table VI
STATE SPACE MODEL COEFFICIENTS

REFERENCES

[1] J. Larminie and A. Dicks, *Fuel Cell Systems Explained*, 2nd ed. John Wiley & Sons Inc, 2003.

[2] C. Kunusch, "Modelling and nonlinear control of pem fuel cell systems," Ph.D. dissertation, Electrical Department, National University of La Plata, March 2009.

[3] J. Pukrushpan, A. Stefanopoulou, and H. Peng, *Control of Fuel Cell Power Systems*. Springer, 2004.

[4] R. Talj, D. Hissel, R. Ortega, M. Becherif, and M. Hilairet, "Experimental validation of a PEM fuel-cell reduced-order model and a moto-compressor Higher Order Sliding-Mode control," *Industrial Electronics, IEEE Transactions on*, vol. 57, no. 6, pp. 1906 – 1913, 2010.

[5] C. Kunusch, P. Puleston, M. Mayosky, and J. Riera, "Sliding mode strategy for PEM fuel cells stacks breathing control using a Super-Twisting algorithm," *IEEE Transactions on Control System Technology*, vol. 17, pp. 167–174, 2009.

[6] W. K. Na and B. Gou, "Feedback-linearization-based nonlinear control for PEM fuel cells," *Energy Conversion, IEEE Transactions on*, vol. 23, no. 1, pp. 179–190, 2008.

[7] J. Zhang, G. Liu, W. Yu, and M. Ouyang, "Adaptive control of the airflow of a PEM fuel cell system," *Journal of Power Sources*, vol. 179, no. 2, pp. 649–659, 2008.

[8] J. Amphlett, R. Baumert, R. Mann, B. Peppley, and P. Roberge, "Performance modelling of the ballard mark iv solid polymer electrolyte fuel cell," *Journal of Electrochemical Society*, vol. 142, no. 1, pp. 9–15, 1995.

[9] T. Springer, T. Zawodzinski, and S. Gottesfeld, "Polymer electrolyte fuel cell model," *Journal of Electrochemical Society*, vol. 138, no. 8, pp. 2334–2342, 1991.

[10] P. Rodatz, "Dynamics of the polymer electrolyte fuel cell: Experiments and model-based analysis," Ph.D. dissertation, Swiss Federal Institute of Technology Zurich, 2003.

[11] F. Grasser and A. Rufer, "A fully analytical PEM fuel cell system model for control applications," *Industry Applications, IEEE Transactions on*, vol. 43, no. 6, pp. 1499–1506, 2007.

[12] F. Gao, B. Blunier, M. Simoes, and A. Miraoui, "Pem fuel cell stack modeling for real-time emulation in hardware-in-the-loop applications," *Energy Conversion, IEEE Transactions on*, vol. PP, no. 99, pp. 1 – 11, 2010.

[13] M. Khan and M. Iqbal, "Modelling and analysis of electro-chemical, thermal, and reactant flow dynamics for a pem fuel cell system," *Fuel cells*, vol. 5, no. 4, pp. 463–475, 2005.

[14] C. Bao, M. Ouyang, and B. Yi, "Modeling and control of air stream and hydrogen flow with recirculation in a pem fuel cell system–i. control-oriented modeling," *International Journal of Hydrogen Energy*, vol. 31, no. 13, pp. 1879–1896, 2006.

[15] C. Kunusch, P. Puleston, M. Mayosky, and A. Dávila, "Efficiency optimisation of an experimental PEM fuel cell system via Super Twisting control," in *11th International Workshop on Variable Structure Systems*, Mexico DF, Mexico., June 2010, pp. 319–324.

[16] J. D'Errico, "Polyfitn (n-d polynomial regression model)," 2006. [Online]. Available: http://www.mathworks.com/matlabcentral/fileexchange

[17] Cellkraft, *P-10 humidifier manual: v 2.0*, 2007.

[18] S. Dutta, S. Shimpalee, and J. Van Zee, "Numerical prediction of mass-exchange between cathode and anode channels in a pem fuel cell," *International Journal of Heat and Mass Transfer*, vol. 44, pp. 2029–2042, 2001.

[19] D. McKay, W. Ott, and A. Stefanopoulou, "Modeling, parameter identification, and validation of reactant and water dynamics for a fuel cell stack," in *ASME International Mechanical Engineering Congress & Exposition*, 2005.

[20] C. Ramos-Paja, C. Bordons, A. Romero, R. Giral, and L. Martinez-Salamero, "Minimum fuel consumption strategy for pem fuel cells," *Industrial Electronics, IEEE Transactions on*, vol. 56, no. 3, pp. 685 – 696, 2009.

[21] C. Kunusch, P. Puleston, M. Mayosky, and J. Moré, "Characterization and experimental results in PEM fuel cell electrical behaviour," *International Journal of Hydrogen Energy*, vol. 35, pp. 5876–5881, 2010.

Cristian Kunusch obtained his Diploma (2003, National University of La Plata, Argentina) in Electronic Engineering, his M.Sc. (2003, National University of La Plata, Argentina) in Engineering and his Ph.D. (2009, National University of La Plata, Argentina) in Engineering and Automation. He is currently an Associate Researcher at the Institut de Robòtica i Informàtica Industrial (CSIC-UPC), Barcelona, Spain. He was Assistant Professor of Automatic Control (2003-2009) at the National University of La Plata, Argentina. His current work addresses the control and automation issues associated with PEM fuel cells systems.

Paul F. Puleston received the B.S.E.E. degree (with first class honors) and the Ph.D. degree from the National University of La Plata, Argentina, in 1988 and 1997, respectively. During 1999-2000, he has been a Research Associate at the Engineering Department, Leicester University, U.K. He is currently Full Professor at the Electrical Engineering Department, National University of La Plata. Dr. Puleston is a Research Member of the National Council for Scientific and Technical Research, Argentina. He was awarded the Gold Medal "Ing. Antonio Marin" of the National Academy of Engineering in 2002. His research interests include automatic control and renewable energy systems.

Miguel A. Mayosky (M97-SM'98) was born in La Plata, Argentina, in 1960. He received the Engineer on Electronics degree (First Class Award) from the University of La Plata (UNLP), La Plata, Argentina, and the Ph.D. in Computer Science from the Autonomous University of Barcelona, Spain (Cum Laude) in 1983 and 1990, respectively. He is currently a Full Professor of Automatic Control Systems at the School of Engineering, UNLP, and also a Member of the Research Staff of the Buenos Aires Scientific Research Commission (CICpBA). Dr. Mayosky was President of the Argentina Chapter of the IEEE Computational Intelligence Society (2005-2006). His research activities involve real-time data acquisition and control systems, instrumentation for High Energy Physics experiments, and embedded computer architectures.

Attila P. Husar is currently a Ph.D. candidate at the Universitat Politcnica de Catalunya (UPC), Barcelona Spain where he has designed and built different PEMFC test stations. He has spent his 14-year engineering career directly involved in development of PEM fuel cells and fuel cell systems. Before returning to school for his Ph.D, he worked at Energy Partners, West Palm Beach, FL. He led fuel cell engineering team that designed and built fuel cells and fuel cell systems and put them in practical applications. He is the author or co-author of more than 20 publications in international scientific journals on fuel cells and conference proceedings. He holds a Bachelors and M.Sc. degree in mechanical engineering from University of Miami (Coral Gables FL., USA).